materials

MDPI

Article

An Exponential Pennes Bioheat Model for Laser Pulse-Induced Heat Transfer in 1D Skin Tissue

Ahlam A. Al-Raezah [1] and Ashraf M. Zenkour [2,*]

[1] Department of Mathematics, College of Science, King Khalid University, Abha 61421, Saudi Arabia; assad@kku.edu.sa
[2] Department of Mathematics, Faculty of Science, King Abdulaziz University, Jeddah 21589, Saudi Arabia
* Correspondence: zenkour@kau.edu.sa

Abstract

A generalized thermoelastic study of skin tissue under laser radiation is presented in this paper using the exponential Pennes thermoelasticity (e-PT) model. Tissue thermal behaviour is examined in relation to blood perfusion and metabolic heat generation. The suggested formulation describes finite-speed heat propagation and the linked thermomechanical response of living tissue by incorporating exponential thermal memory into the conventional Pennes bioheat equation. The Laplace transform is exploited to justify the governing equations methodically. The transient temperature, displacement, dilatation, and stress fields are obtained by numerically inverting the transformed solutions. The effects of thermoelastic theory, cooling heat transfer coefficient, laser radiation exposure duration, and time on the mechanical and thermal reactions of skin tissue are examined numerically. The findings show that compared to the classical, simple, and refined Pennes models, the exponential Pennes model predicts higher thermo-mechanical coupling and more noticeable thermal-wave propagation.

Keywords: exponential PT; biological skin tissue; laser pulse

1. Introduction

The majority of research on non-Fourier biothermal transfer, according to a review of the literature, uses numerical techniques. On the other hand, the current work provides exact temperature distributions in skin tissue by developing analytic solutions for both Fourier and non-Fourier biothermal equations. These analytical findings provide more physical understanding and are trustworthy standards for verifying numerical models. Shih et al. [1] used the Laplace transform and Pennes bioheat equation to analytically examine the temperature behaviour of semi-infinite living tissue under sinusoidal surface heating. The thermal wave and Pennes bioheat models under laser irradiation were analytically solved for various albedo levels by Ahmadikia et al. [2]. Kundu and Debojit [3] used the Laplace transform method to examine Fourier and non-Fourier thermal responses in 1D skin tissue.

A simplified 1D spherical bioheat model based on the Pennes equation was created by Kengne and Lakhssassi [4]. For immediate skin heating, Askarizadeh and Ahmadikia [5] provided precise systematic solutions to 2D Fourier and non-Fourier biothermal equations. Majchrzak et al. [6] used generalized dual phase-lag (DPL) equations to

Academic Editor: Zine El Abiddine Fellah

Received: 31 October 2026
Revised: 20 November 2026
Accepted: 23 November 2026
Published: 24 November 2026

Copyright: © 2026 by the authors. Licensee MDPI, Basel, Switzerland. This article is an open access article distributed under the terms and conditions of the Creative Commons Attribution (CC BY) license.

quantitatively describe multilayer skin heating. To forecast heat distributions and current damage in skin tissues, Kabiri and Talaee [7] developed a solution of the hyperbolic Pennes biothermal equation. Based on the Pennes equation for bioheat analysis, Mukaddes et al. [8] created a 3D finite element simulation of skin tissue. Using electromagnetic wave propagation, Sadeghi et al. [9] studied the photothermal behaviour of a four-layer skin model under various light intensities and wavelengths. Heat transport predictions from thermal wave and Pennes bioheat models in a two-dimensional multilayer skin were compared by Tasnim and Nasrin [10]. Akulova and Sheremet [11] used the Pennes bioheat model to simulate transient bioheat transmission in five-layer biological tissue containing a tumour.

By adding fractional-order derivatives to account for memory and genetic influences in skin tissues, the fractional Pennes bioheat model expands upon the conventional Pennes equation. Consequently, it enhances the calculation of transient temperature distributions during thermal treatments and laser heating and offers a further explanation of non-Fourier thermal transport. A fractional Pennes biothermal model is exploited by Ezzat et al. [12] to analyze heat transmission in live tissue under immediate surface heating. The fractional Pennes equation for biological tissue under Dirichlet, Neumann, and Robin boundary conditions is solved analytically by Cui et al. [13]. By imposing temperature and heat flux continuity at interfaces, Sarkar et al. [14] provided an analytical steady-state solution of the multilayer Pennes biothermal equation. A time-fractional Pennes model with temperature-dependent perfusion and finite/infinite heat propagation speeds was presented by Ferrás et al. [15]. To better forecast heating and cooling processes, Yang and Sun [16] created a space-fractional Pennes simulation to explain non-Fourier thermal conduction in skin tissue. For skin exposed to thermal stress, Tian et al. [17] developed a fractional version of the Kelvin–Voigt thermoviscoelastic theory combined with fractional Pennes biothermal conduction. To explore the coupled thermoelastic behaviour of skin tissue, Tian et al. [18] expanded this framework by adding temperature-dependent thermal characteristics and fractional PL bioheat conduction.

The DPL bioheat theory is employed by Askarizadeh and Ahmadikia [19] to examine transient heat transmission in biological tissue under periodic and pulse-train heating. Kumar et al. [20] computationally investigated a DPL model with blood perfusion in recurring heat flux, whereas Kumar and Rai [21] investigated a time-fractional DPL model including metabolic and electromagnetic thermal sources. Zhang et al. [22] developed a triple-phase-lag (TPL) bioheat theory for skin tissue, while Zhang et al. [23] investigated laser-induced thermoelastic reactions using a generalized DPL model. Wang et al. [24] and Al-Lehaibi [25] reported on the effects of a moving heat source and continuous surface heating, respectively, while Rani et al. [26] employed a generalized DPL thermoelastic model to computationally study wave propagation in biological tissue with voids. Salem et al. [27] suggested a fractional DPL theory created on the Atangana–Baleanu derivative to account for the temperature-dependent thermophysical properties of skin tissue. Abbas et al. [28] presented a study of the thermoelastic behaviour of instantaneously heated skin tissue. Parmar et al. [29] used the two-temperature and generalized thermoelastic analyses.

A Moore–Gibson–Thompson (MGT)-based bioheat model is developed by Megahid et al. [30] to better forecast temperature evolution and characterize thermal conduction in skin tissue. The fourth-order MGT theory is used by Abouelregal et al. [31] and Megahid [32] to study the biothermal response of skin tissue subjected to variable thermal loading and electromagnetic radiation. Applying a modified MGT model with various time derivatives under ramp-type heating, Bhattacharya and Kanoria [33] examined the thermoelastic response of a thin skin layer. Via Pennes bioheat model, Eringen's nonlocal elasticity,

and fourth-order MGT thermoelasticity, Mondal et al. [34] investigated the thermoelastic behaviour of three-layer skin tissue exposed to a moving thermal source.

This paper presents a generalized thermoelastic investigation of laser-exposed skin tissue using the exponential Pennes thermoelasticity (e-PT) model. Tissue thermal behavior is investigated in connection with blood perfusion and metabolic heat production. The proposed formulation addresses finite-speed heat propagation and the related thermomechanical response of skin tissue by integrating exponential thermal memory into the standard Pennes bioheat equation. The Laplace transform is used to provide an analytical explanation for the governing equations. The transient temperature, displacement, dilatation, and stress fields are calculated numerically by inverting the converted solutions. The effects of thermoelastic theory, cooling heat transfer coefficient, laser radiation exposure duration, and time on the mechanical and thermal reactions of skin tissue are examined numerically. The results show that the exponential Pennes model has a larger thermomechanical coupling effect and more prominent thermal-wave propagation than the classical, simple, and refined Pennes models. This behaviour can be explained physically by the exponential time-memory operator, which does not just describe the thermal response through instantaneous or finite-order relaxation effects, but also takes into account the cumulative influence of the thermal history. As a result, the thermal response shows more pronounced wave-like features, such as variations in wave attenuation, propagation speed, and amplitude. These findings imply that delayed heat transmission and its relationship to tissue deformation and induced stresses in skin tissue can be better mathematically described by exponential memory.

2. Basic Equations

Consider in Figure 1 a thermoelastic lamina of human skin tissue ($0 \leq z \leq h$) at the environment (arterial blood) temperature T_b to study changes in field variables of a biological tissue. The upper surface ($z = 0$) of the tissue layer is cooled, while the lower surface remains insulated. There is no stress on either surface. Assume that the upper layer of the tissue is uniformly exposed to a normal laser beam; some of the radiation will be transmitted, while the rest will be reflected. Because of the laser beam's uniform incidence, the problem will be addressed as a one-dimensional problem, with all variables being functions of z and t.

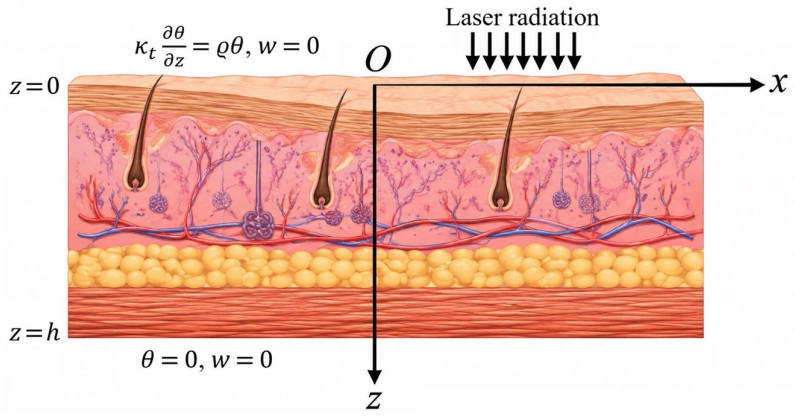


Figure 1. A schematic description of biological skin tissue.

The displacements are explained as

$$u_x = u_y = 0, \qquad u_z = w(z,t), \tag{1}$$

where w is the displacement (axial deflection). All strains have gone, excluding the corresponding one

$$\varepsilon_z = \frac{\partial w(z,t)}{\partial z}, \tag{2}$$

which is the same as the cubic dilatation $\varepsilon = \varepsilon_z$.

The coupled bio-heat conduction equation for strain and temperature variations is consistent with a modified version of the Lord and Shulman thermoelasticity theory [35,36] as well as Pennes' bioheat equation. When metabolic heat generation occurs, the refined Pennes bioheat theory (r-PT)

$$\kappa_t \frac{\partial^2 \theta}{\partial z^2} = \mathcal{D}\left[\frac{\partial}{\partial t}(\rho_t c_t \theta + \gamma_t T_b \varepsilon) - Q\right], \tag{3}$$

where κ_t and c_t denote the tissue's thermal conductivity and thermal capacity of a unit mass, $\theta = T - T_b$ is the thermodynamic temperature change in the tissues (where T is the absolute temperature) and ρ_t is the tissue mass density. The heat modulus, $\gamma_t = (2\mu_t + 3\lambda_t)\alpha_t$, is calculated using Lamé's constants λ_t and μ_t, and the thermal expansion coefficient is denoted as α_t. The parameter $\mathcal{D}$ represents the time-derivative operator:

$$\mathcal{D} = 1 + \sum_{n=1}^{N} \frac{\tau^n}{n!} \frac{\partial^n}{\partial t^n}, \quad N \geq 1, \tag{4}$$

where τ and Q represent the relaxation time and heat source for the skin tissue. In fact, Q has been significantly employed in different kinds of research, including [37–39]. It is described as

$$Q = \omega_b \rho_b c_b (T_b - T) + Q_m + Q_L, \tag{5}$$

where ω_b, ρ_b, and c_b represent blood perfusion rate, density of blood mass, and specific heat, while Q_m and Q_L denote a metabolic heat source in tissue cells and external laser radiation.

The first model of biological tissues that is developed by Pennes based on Fourier's law of heat conduction is obtained from Equation (3) by setting $\mathcal{D} = 1$ as

$$\kappa_t \frac{\partial^2 \theta}{\partial z^2} = \frac{\partial}{\partial t}(\rho_t c_t \theta + \gamma_t T_b \varepsilon) + \omega_b \rho_b c_b \theta - Q_m - Q_L, \tag{6}$$

which is also denoted as the classical Pennes thermoelasticity theory (c-PT) for bioheat tissues. Also, the simple Pennes generalized thermoelasticity theory (s-PT) is obtained from Equation (3) by setting $N = 1$ as

$$\kappa_t \frac{\partial^2 \theta}{\partial z^2} = \left(1 + \tau \frac{\partial}{\partial t}\right)\left[\frac{\partial}{\partial t}(\rho_t c_t \theta + \gamma_t T_b \varepsilon) + \omega_b \rho_b c_b \theta - Q_m - Q_L\right]. \tag{7}$$

In addition, the refined Pennes generalized thermoelasticity theory (r-PT) is obtained from Equation (3) by setting $N > 1$ as

$$\kappa_t \frac{\partial^2 \theta}{\partial z^2} = \left(1 + \tau \frac{\partial}{\partial t} + \frac{\tau^2}{2!}\frac{\partial^2}{\partial t^2} + \cdots\right)\left[\frac{\partial}{\partial t}(\rho_t c_t \theta + \gamma_t T_b \varepsilon) + \omega_b \rho_b c_b \theta - Q_m - Q_L\right]. \tag{8}$$

The most novel and important Pennes generalized thermoelasticity theory is obtained from Equation (3) by setting $N \to \infty$ [40]. That is,

$$\kappa_t \frac{\partial^2 \theta}{\partial z^2} = e^{\tau_q \frac{\partial}{\partial t}}\left[\frac{\partial}{\partial t}(\rho_t c_t \theta + \gamma_t T_b \varepsilon) + \omega_b \rho_b c_b \theta - Q_m - Q_L\right], \tag{9}$$

which is said to be the exponential Pennes generalized thermoelasticity theory (e-PT). The laser radiation Q_L takes the form [41,2]

$$Q_L = \mu_a f(t)\left(C_1 e^{-\frac{k_1 z}{\delta}} - C_2 e^{-\frac{k_2 z}{\delta}}\right), \tag{10}$$

where μ_a represents the absorption coefficient, $f(t)$ represents the incident laser irradiance, and δ denotes the effective optical penetration depth [42],

$$\delta = \frac{1}{\sqrt{3\mu_a[\mu_a+\mu_s(1-g)]}}, \tag{8}$$

in which g and μ_a denote the anisotropy factor and scattering coefficient. Additionally, the diffuse reflectance of light at the irradiated surface R_d determines C_1, C_2, k_1, and k_2, which can be derived from Monte Carlo solutions as follows [43]:

$$\begin{gathered} C_1 = 3.09 + 5.44R_d - 2.12e^{-21.5R_d}, \\ C_2 = 2.09 - 1.47R_d - 2.12e^{-21.5R_d}, \\ k_1 = 1 - \left(1 - \sqrt{3}\right)e^{-20.1R_d}, \\ k_2 = 1.63e^{3.4R_d}. \end{gathered} \tag{12}$$

If the layer is subjected to laser radiation of intensity q_0, which is activated after a delay time α. Its temporal variation is described using the Heaviside unit step function $H(\cdot)$ as follows

$$g(t) = q_0 H(t)H(t-\alpha). \tag{93}$$

The dynamic equation regulating the skin tissue can be formulated as

$$\frac{\partial \sigma}{\partial z} = \rho_t \frac{\partial^2 w}{\partial t^2}, \tag{10}$$

and the normal stress is expressed as

$$\sigma = \sigma_z = (\lambda_t + 2\mu_t)\varepsilon - \gamma_t \theta. \tag{11}$$

It is possible to introduce the problem's initial and boundary conditions here. The starting circumstances of the subject at hand are thought to be

$$\theta(z,t)|_{t=0} = \left.\frac{\partial^n \theta(z,t)}{\partial t^n}\right|_{t=0} = 0, \qquad w(z,t)|_{t=0} = \left.\frac{\partial^n w(z,t)}{\partial t^n}\right|_{t=0} = 0, \qquad n \geq 1. \tag{12}$$

The skin tissue is mechanically clamped on both the upper and lower surfaces. The laser thermal loading is applied at the upper surface ($z = 0$), where convective heat exchange with the surrounding environment is also considered. The lower surface ($z = h$) is maintained at the reference temperature. Accordingly, the thermal and mechanical boundary conditions are expressed as

$$\kappa_t \left.\frac{\partial \theta}{\partial z}\right|_{z=0} = \varrho\theta(0,t), \qquad \theta(h,t) = 0, \qquad w(0,t) = 0, \qquad w(h,t) = 0. \tag{13}$$

where $\varrho > 0$ is the cooling heat transfer coefficient at $z = 0$.

3. Solution to the Problem

Now, using Equation (15) in Equation (14) with the aid of Equation (2) yields

$$\frac{\partial^2 w}{\partial z^2} - b_1 \frac{\partial \theta}{\partial z} = b_2 \frac{\partial^2 w}{\partial t^2}, \tag{14}$$

where

$$b_1 = \frac{\gamma_t}{\lambda_t + 2\mu_t}, \qquad b_2 = \frac{\rho_t}{\lambda_t + 2\mu_t}. \tag{15}$$

Also, the heat conduction equation in its final form is given by

$$\frac{\partial^2 \theta}{\partial z^2} = \mathcal{D}\left[\frac{\partial}{\partial t}\left(b_3\theta + b_4\frac{\partial w}{\partial z}\right) + b_5\theta - Q_1 - H(t)H\left(t - \tau_p\right)\left(b_6 \mathrm{e}^{-\frac{k_1 z}{\delta}} - b_7 \mathrm{e}^{-\frac{k_2 z}{\delta}}\right)\right], \tag{16}$$

where

$$b_3 = \frac{\rho_t c_t}{\kappa_t}, \quad b_4 = \frac{\gamma_t T_b}{\kappa_t}, \quad b_5 = \frac{\omega_b \rho_b c_b}{\kappa_t}, \quad b_6 = \frac{C_1 q_0 \mu_a}{\kappa_t}, \quad b_7 = \frac{C_2 q_0 \mu_a}{\kappa_t}, \quad Q_1 = \frac{Q_m}{\kappa_t}. \tag{17}$$

Equations (18) and (20) show that the important unknowns are deflection w and temperature θ. The first equation shows how temperature affects deflection, whereas the second equation shows how strain affects temperature in the other direction.

The Laplace transform, as is well known, may turn any time function into a complex parameter s. It is described as

$$\mathcal{L}\{f(z,t)\} = \bar{f}(z,s) = \int_0^\infty \mathrm{e}^{-st} f(z,t)\mathrm{d}t. \tag{18}$$

By transforming the partial differential equations into ordinary differential equations in the s-domain, this transformation makes them simpler. The governing formulas become

$$\frac{\mathrm{d}^2\bar{w}}{\mathrm{d}z^2} - 2c_1\bar{w} = b_1\frac{\mathrm{d}\bar{\theta}}{\mathrm{d}z}, \tag{19}$$

$$\frac{\mathrm{d}^2\bar{\theta}}{\mathrm{d}z^2} - 2c_2\bar{\theta} - 2c_3\frac{\mathrm{d}\bar{w}}{\mathrm{d}z} = -b_8\mathrm{e}^{-\bar{k}_1 z} + b_9\mathrm{e}^{-\bar{k}_2 z} - Q_2, \tag{24}$$

where

$$c_1 = \frac{b_2 s^2}{2}, \quad c_2 = \frac{1}{2}\varpi(b_3 s + b_5), \quad c_3 = \frac{1}{2}\varpi b_4 s, \quad b_8 = \frac{\varpi b_6 e^{-s\tau p}}{s}, \quad b_9 = \frac{\varpi b_7 e^{-s\tau p}}{s}, \quad \bar{k}_1 = \frac{k_1}{\delta}, \quad \bar{k}_2 = \frac{k_2}{\delta}, \quad Q_2 = \frac{Q_1}{s}, \quad \varpi = 1 + \sum_{n=1}^{N}\frac{(s\tau)^n}{n!}. \tag{205}$$

When $N \to \infty$, one gets $\varpi = \mathrm{e}^{s\tau}$.

The general solutions of the system of Equations (23) and (24) are

$$\bar{w} = c_4\sum_{j=1}^{2}\left(A_j\mathrm{e}^{\zeta_j z} + B_j\mathrm{e}^{-\zeta_j z}\right) + c_6\mathrm{e}^{-\bar{k}_1 z} - c_7\mathrm{e}^{-\bar{k}_2 z}, \tag{21}$$

$$\bar{\theta} = c_5\sum_{j=1}^{2}\beta_j\left(A_j\mathrm{e}^{\zeta_j z} - B_j\mathrm{e}^{-\zeta_j z}\right) + c_8\mathrm{e}^{-\bar{k}_1 z} - c_9\mathrm{e}^{-\bar{k}_2 z} + Q_3, \tag{27}$$

where A_j and B_j are four integration constants, ζ_j are the roots of the characteristic equation

$$\zeta^4 - 2(b_1c_3 + c_1 + c_2)\zeta^2 + 4c_1c_2 = 0, \tag{22}$$

and

$$\zeta_{1,2}^2 = b_1c_3 + c_1 + c_2 \pm \zeta_0, \qquad \zeta_0^2 = b_1^2c_3^2 + 2b_1c_3(c_1 + c_2) + (c_1 - c_2)^2\,, \tag{23}$$

in addition to

$$\beta_j = \frac{\zeta_0 \pm (b_1c_3 - c_1 + c_2)}{\zeta_j}, \quad c_4 = \frac{k_3k_4}{(k_5^2 - \zeta_0^2)(k_6^2 - \zeta_0^2)}, \quad c_5 = \frac{c_4}{b_1}, \quad c_6 = \frac{b_1b_8c_4\bar{k}_1}{k_3}, \quad c_7 = \frac{b_1b_9c_4\bar{k}_2}{k_4}, \quad c_8 = \frac{b_8c_4(2c_1 - \bar{k}_1^2)}{k_3}, \quad c_9 = \frac{b_9c_4(2c_1 - \bar{k}_2^2)}{k_4}, \quad Q_3 = \frac{c_4Q_2}{2c_2}. \tag{24}$$

Finally, the dilatation and stress of the tissue are given as

$$\bar{\varepsilon}(z,s) = c_4\sum_{j=1}^{2}\zeta_j\left(A_j\mathrm{e}^{\zeta_j z} - B_j\mathrm{e}^{-\zeta_j z}\right) - c_6\bar{k}_1\mathrm{e}^{-\bar{k}_1 z} + c_7\bar{k}_2\mathrm{e}^{-\bar{k}_2 z}, \tag{25}$$

$$\bar{\sigma}(z,s) = \sum_{j=1}^{2}\psi_j\left(A_j\mathrm{e}^{\zeta_j z} - B_j\mathrm{e}^{-\zeta_j z}\right) - k_7\mathrm{e}^{-\bar{k}_1 z} + k_8\mathrm{e}^{-\bar{k}_2 z} - \gamma_t Q_3, \tag{32}$$

where

$$\psi_j = (\lambda_t + 2\mu_t)\zeta_j c_4 - \beta_j\gamma_t c_5, \qquad k_7 = (\lambda_t + 2\mu_t)c_6\bar{k}_1 + \gamma_t c_8, \qquad k_8 = (\lambda_t + 2\mu_t)c_7\bar{k}_2 + \gamma_t c_9. \tag{26}$$

The boundary conditions in Equation (17) are applied to the analytical solutions in Equations (26) and (27) to derive the unknown integration constants A_j and B_j. That is,

$$\kappa_t c_5 \sum_{j=1}^{2} \beta_j \zeta_j (A_j + B_j) - \varrho c_5 \sum_{j=1}^{2} \beta_j (A_j - B_j) = \kappa_t (c_8 \bar{k}_1 - c_9 \bar{k}_2) + \varrho (Q_3 + c_8 - c_9),$$
$$c_5 \sum_{j=1}^{2} \beta_j (A_j e^{\zeta_j h} - B_j e^{-\zeta_j h}) = c_9 \bar{k}_2 - c_8 \bar{k}_1 - Q_3, \quad (274)$$
$$c_4 \sum_{j=1}^{2} (A_j e^{\zeta_j h} + B_j e^{-\zeta_j h}) = c_7 \bar{k}_2 - c_6 \bar{k}_1,$$
$$c_4 \sum_{j=1}^{2} (A_j + B_j) = c_7 - c_6.$$

So, the integration parameters A_j and B_j can be obtained by solving the above system of four equations.

4. Numerical Outcomes and Discussions

Once the governing equations in the transformed domain have been explained, the original time-dependent solution can be recovered utilizing the inverse Laplace transform. The Laplace transform can be numerically inverted utilizing the Fourier-series approach (Dubner and Abate [44]). For a fixed x, the function $\bar{f}(x,s)$ denotes the Laplace transform of $f(x,t)$. The inverse Laplace transform $f(x,t)$ can be estimated as

$$f(x,t) = \frac{e^{ct}}{t}\left[\frac{1}{2}\bar{f}(x,c) + \sum_{m=1}^{M}(-1)^m \mathrm{Re}\left\{\bar{f}\left(x, c + \frac{im\pi}{t}\right)\right\}\right], \quad (28)$$

where M is a truncation number high enough to control accuracy, Re stands for the real part, and $i = \sqrt{-1}$. A positive real constant, c, is selected so that it lies to the right of every singularity of $\bar{f}(x,s)$ (preferably, $ct \approx 4.7$ for faster convergence). For Laplace transforms, the aforementioned formula is a well-known and trustworthy numerical inversion method that works especially well for dynamic thermoelastic issues where analytical inversion is challenging.

Table 1 presents a list of the thermophysical features of blood and biological tissue [13,40]. The thickness of the skin tissue is assumed to be $h = 4$ mm. Other biothermoelastic constants are reported in Table 1. The values of temperature ($\hat{\theta} = 10 \times \theta$), displacement ($\hat{w} = 10^8 \times w$), volumetric strain ($\hat{\varepsilon} = 10^5 \times \varepsilon$), and axial stress ($\hat{\sigma} = 10^{-4} \times \sigma$) are expressed. The numerical results are presented and examined in detail in Figures 2–13.

Table 1. Thermophysical features of blood and biological tissue.

Feature	Value	Unit
Lame's constant λ_t	8.27×10^8	kg/(m · s^2)
Lame's constant μ_t	3.446×10^7	kg/(m · s^2)
Density ρ_t	1190	kg/m^3
Tissue's specific heat c_t	3600	J/(K · kg)
Thermal conductivity k_t	0.235	W/(m · K)
Blood density ρ_b	1060	kg/m^3
Blood's specific heat c_b	3770	J/(K · kg)
Linear thermal expansion α_t	1×10^{-4}	1/K
Arterial blood temperature T_b	310	K
Rate of blood perfusion ω_b	1.87×10^{-3}	1/s
Metabolic heat source Q_m	368.1	W/m^3
Cooling heat transfer coefficient ϱ	100	W/(m^2 · K)

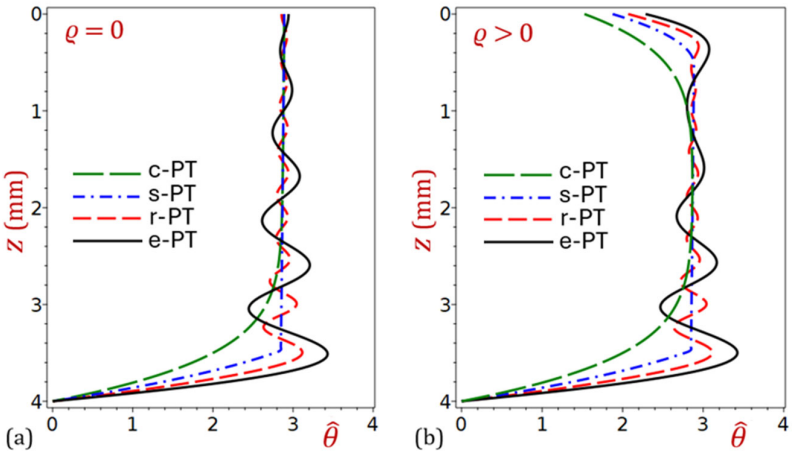


Figure 2. Distribution of temperature $(\hat{\theta})$ throughout the skin tissue utilizing numerous theories with (**a**) $\varrho = 0$ and (**b**) $\varrho > 0$.

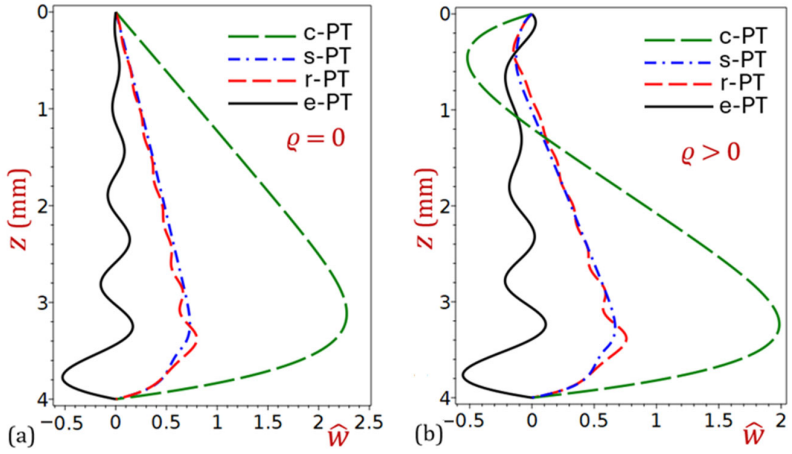


Figure 3. Distribution of axial displacement $(\hat{w})$ throughout the skin tissue employing numerous theories with (**a**) $\varrho = 0$ and (**b**) $\varrho > 0$.

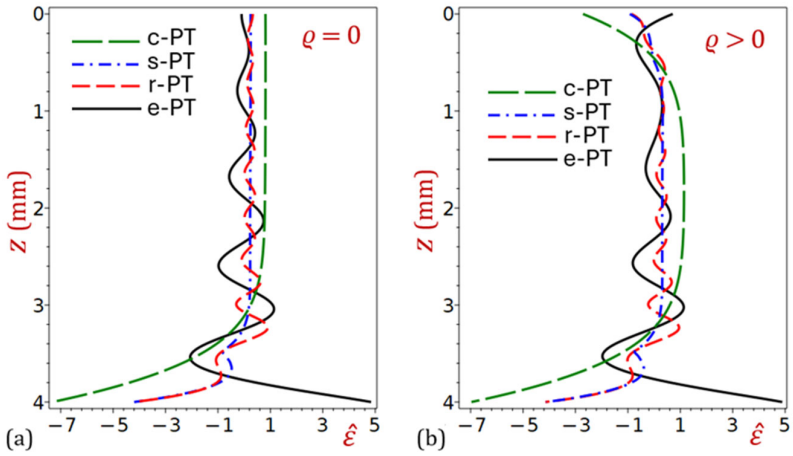


Figure 4. Distribution of dilatation $(\hat{\varepsilon})$ throughout the skin tissue utilizing numerous theories with (**a**) $\varrho = 0$ and (**b**) $\varrho > 0$.

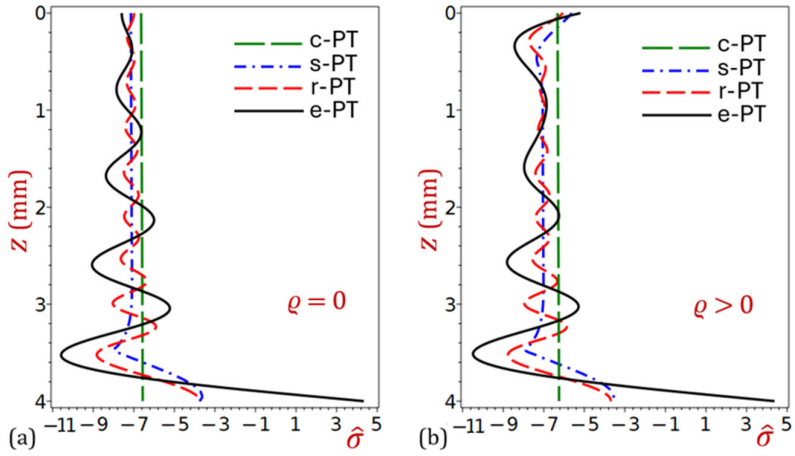


Figure 5. Distribution of axial stress $(\hat{\sigma})$ throughout the skin tissue employing numerous theories with (**a**) $\varrho = 0$ and (**b**) $\varrho > 0$.

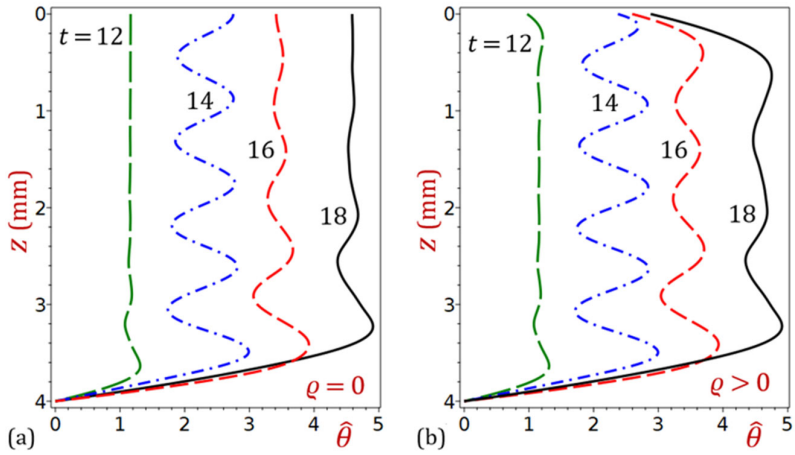


Figure 6. Impact of time t on the temperature $(\hat{\theta})$ throughout the skin tissue utilizing e-PT with (**a**) $\varrho = 0$ and (**b**) $\varrho > 0$.

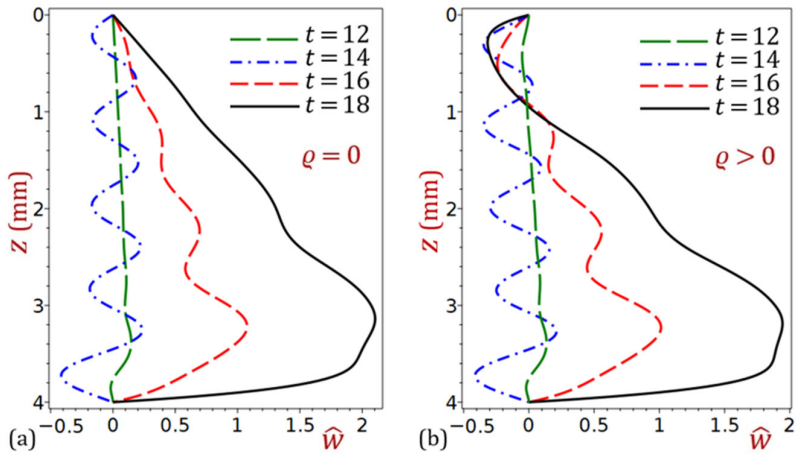


Figure 7. Impact of time t on the displacement $(\hat{w})$ throughout the skin tissue employing e-PT with (**a**) $\varrho = 0$ and (**b**) $\varrho > 0$.

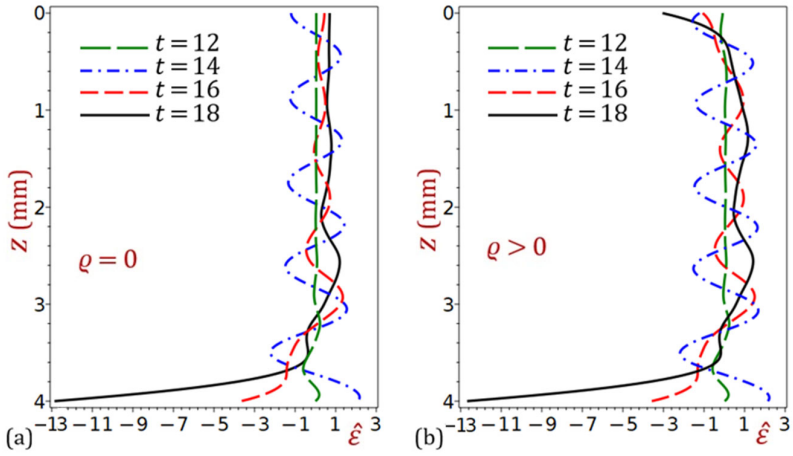


Figure 8. Impact of time t on the dilatation $(\hat{\varepsilon})$ through the skin tissue utilizing e-PT with (**a**) $\varrho = 0$ and (**b**) $\varrho > 0$.

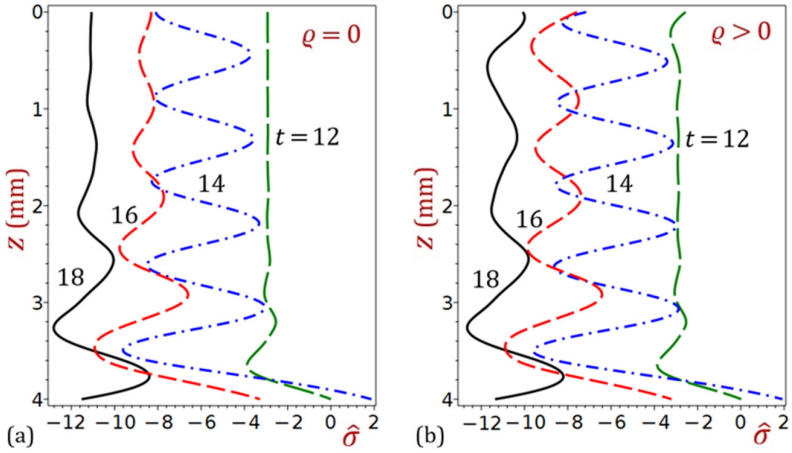


Figure 9. Impact of time t on the axial stress $(\hat{\sigma})$ through the skin tissue employing e-PT with (**a**) $\varrho = 0$ and (**b**) $\varrho > 0$.

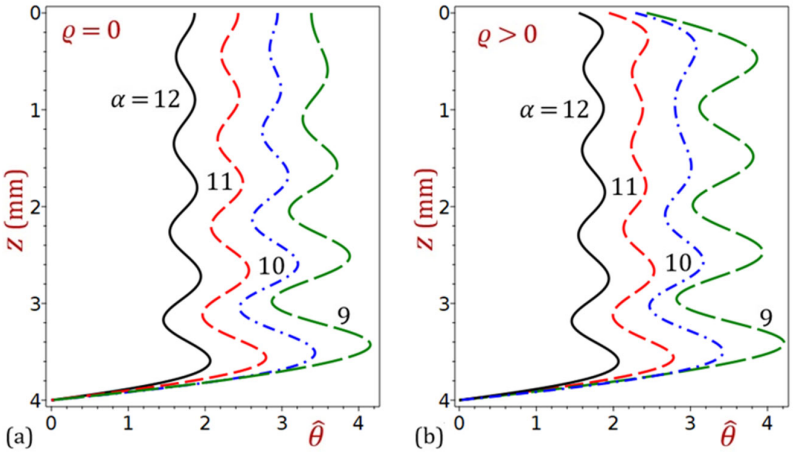


Figure 10. Impact of exposure time α on the temperature $(\hat{\theta})$ through the skin tissue via e-PT with (**a**) $\varrho = 0$ and (**b**) $\varrho > 0$.

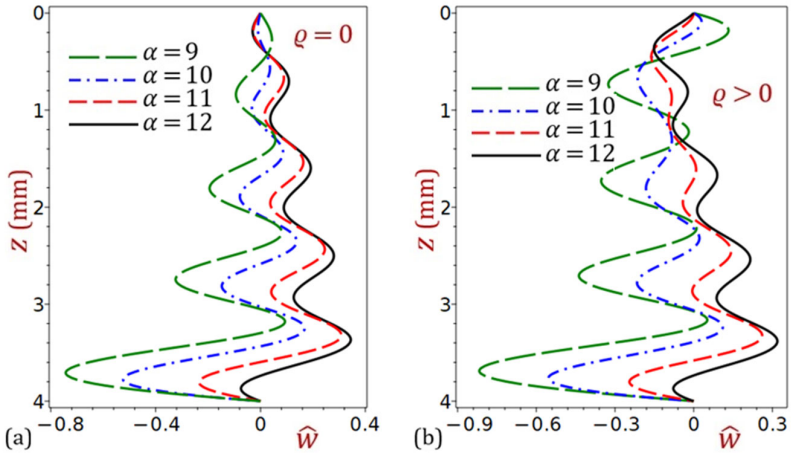


Figure 11. Impact of exposure time α on the axial displacement $(\hat{w})$ through the skin tissue via e-PT with (**a**) $\varrho = 0$ and (**b**) $\varrho > 0$.

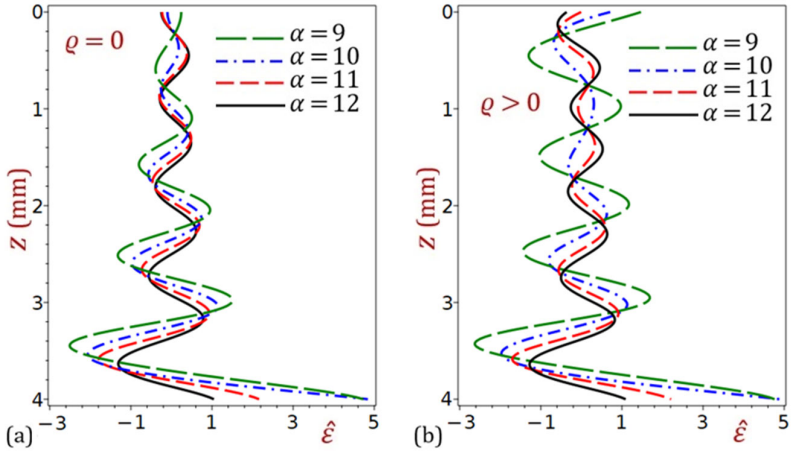


Figure 12. Impact of exposure time α on the dilatation $(\hat{\varepsilon})$ through the skin tissue via e-PT with (**a**) $\varrho = 0$ and (**b**) $\varrho > 0$.

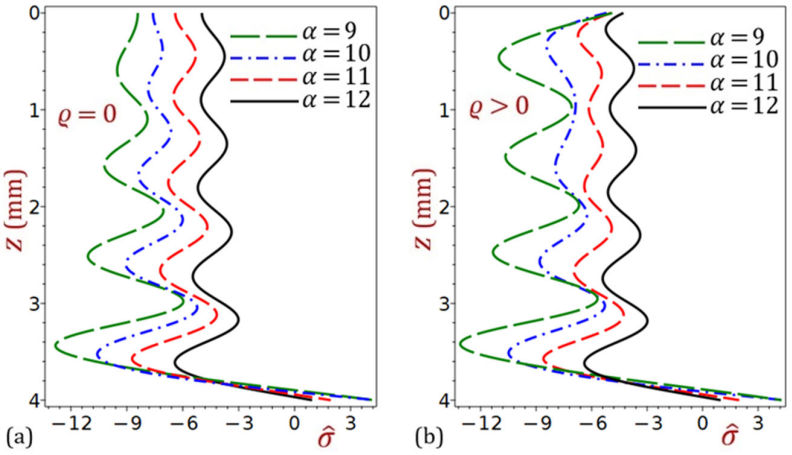


Figure 13. Impact of exposure time α on the axial stress $(\hat{\sigma})$ through the skin tissue via e-PT with (**a**) $\varrho = 0$ and (**b**) $\varrho > 0$.

4.1. Pennes Theory: Simple, Refined, and Exponential Models

Figures 2–5 exhibit the field quantities resulting from numerous coupling theories with fixed relaxation times $\tau = 5$ s, exposure time of laser radiation $\alpha = 10$ s, and time $t = 15$ s.

For four Pennes thermoelasticity theories, Figure 2 compares the dimensionless temperature ($\hat{\theta}$) through the skin thickness ($0 \le z \le 4$) in two boundary conditions: (a) $\varrho = 0$ (no cooling at the upper surface) and (b) $\varrho > 0$ (surface cooling). In both situations, the temperature rises in the vicinity of the lower surface ($z = 4$), where the thermal loading is applied, and falls in the direction of the upper surface ($z = 0$). The exponential theory (e-PT) shows oscillatory behaviour with a somewhat higher temperature over much of the tissue depth, while the classical (c-PT), simple (s-PT), and refined (r-PT) theories predict identical, smooth temperature distributions when $\varrho = 0$. The cooling heat transfer coefficient dramatically lowers the temperature close to the upper surface when $\varrho > 0$, creating a sharper temperature gradient throughout the tissue. The c-PT model has the strongest cooling impact, whereas the e-PT model has the weakest. The exponential hypothesis predicts the biggest departure from the other models, suggesting that adding exponential thermal memory modifies the skin tissue's heat propagation properties.

For the four Pennes thermoelasticity theories under (a) $\varrho = 0$ and (b) $\varrho > 0$, Figure 3 shows the change in the dimensionless axial displacement ($\hat{w}$) over the skin tissue. The greatest positive axial displacement is predicted by the classical Pennes theory (c-PT) over the majority of the tissue thickness, peaking close to the lower surface ($z \approx 3 - 3.5$ mm). Compared to classical theory, the displacement profiles produced by the simple (s-PT) and refined (r-PT) theories are significantly smaller. The impact of exponential thermal memory on the thermo-mechanical response is demonstrated by the non-monotonic, oscillating displacement distribution of the exponential theory (e-PT). The displacement predicted by the classical theory is reduced, and the distributions of the generalized theories are slightly altered, especially in the vicinity of the upper surface ($z = 0$), when the cooling heat transfer coefficient ($\varrho > 0$) is introduced. The exponential model's oscillating behaviour is still visible.

Figure 4 shows the fluctuation in the dimensionless dilatation ($\hat{\varepsilon}$) over the skin tissue for the four Pennes thermoelasticity theories under (a) $\varrho = 0$ and (b) $\varrho > 0$. While the basic (s-PT) and refined (r-PT) theories show comparable distributions with lesser magnitudes, the classical Pennes theory (c-PT) predicts the biggest compressive dilatation near the lower surface ($z = 4$) in the absence of surface cooling ($\varrho = 0$). Because of the impact of exponential thermal memory on the volumetric deformation, the exponential Pennes theory (e-PT) generates an oscillating dilatation profile over the tissue thickness. For both theories, the dilatation decreases close to the upper surface ($z = 0$) when the cooling heat transfer coefficient ($\varrho > 0$) is applied, but the overall distributions stay qualitatively comparable. The classical model exhibits the strongest cooling effect, whereas the generalized models, especially the exponential theory, maintain their distinctive reaction with relatively little modification.

Figure 5 shows how the normalized axial stress ($\hat{\sigma}$) varies with skin tissue thickness under two boundary conditions, (a) $\varrho = 0$ (no cooling) and (b) $\varrho > 0$ (surface cooling), for four Pennes thermoelastic theories. The oscillating stress-wave behaviour is not captured by the classical Pennes theory (c-PT), which predicts almost constant compressive stress throughout the tissue. Thermal relaxation introduces finite-speed thermoelastic wave propagation, which is reflected in the oscillatory stress distributions of the simple (s-PT), refined (r-PT), and exponential (e-PT) theories. The exponential Pennes theory (e-PT) has the strongest memory and wave effects among the generalized theories, producing the largest stress amplitudes and the most noticeable oscillations, especially in the deeper tissue region ($z \approx 3 - 4$ mm). The basic Pennes theory (s-PT) produces the

smallest oscillatory amplitudes, whereas the refined Pennes theory (r-PT) predicts intermediate behaviour. While the broad trends of the four theories do not change, the introduction of surface cooling ($\varrho > 0$) marginally modifies the stress distribution near the upper surface ($z = 0$) and decreases the oscillation amplitudes when compared to the case without cooling.

4.2. The Impact of the Thermal Relaxation Times

We consider the impact of time on the distributions of all variables for e-PT of thermoelasticity in Figures 6–9 ($\tau = 5$ s, $\alpha = 10$ s).

Figure 6 displays how time influences the normalized temperature ($\hat{\theta}$) over the thickness of skin tissue using the exponential Pennes thermoelastic theory (e-PT) for (a) $\varrho = 0$ and (b) $\varrho > 0$. As time passes from $t = 12$ to $t = 18$, the temperature increases throughout the skin tissue, demonstrating the slow accumulation and dissemination of thermal energy. The temperature's wave-like spatial distribution reflects the finite-speed heat propagation expected by the exponential Pennes model. Temperatures are highest at the latest time ($t = 18$) and lowest at the earliest period ($t = 12$). While the overall temperature profiles stay the same, the introduction of surface cooling ($\varrho > 0$) somewhat reduces the temperature near the upper surface ($z = 0$) and diminishes the thermal response in comparison to the case without cooling. In both situations, the deeper tissue region ($z \approx 3 - 4$ mm), where the laser-induced heat builds up, is where the temperature reaches its greatest values.

Figure 7 illustrates how time influences the normalized displacement ($\hat{w}$) through the skin tissue using the exponential Pennes thermoelastic theory (e-PT) for (a) $\varrho = 0$ and (b) $\varrho > 0$. The displacement varies significantly over time, indicating that the laser heating-induced thermo-mechanical reaction is transient. At the beginning ($t = 12$), the displacement is quite small, but over time, it becomes more apparent and achieves its maximum positive values at $t = 18$. The displacement profiles show wave-like behaviour, which is consistent with the exponential Pennes model's prediction of finite-speed thermoelastic wave propagation. Near the lower surface ($z = 4$ mm), the displacement approaches zero, while it reaches its highest value in the deeper part of the tissue ($z \approx 3 - 3.5$ mm). The displacement amplitudes are slightly decreased when surface cooling is introduced ($\varrho > 0$), especially close to the upper surface, but the general shape and temporal evolution essentially stay the same.

Figure 8 illustrates the appearance of time on the normalized dilatation ($\hat{\varepsilon}$) over the skin tissue applying the exponential Pennes thermoelastic theory (e-PT) for (a) $\varrho = 0$ and (b) $\varrho > 0$. The dilatation's discernible oscillating distribution throughout the tissue illustrates the transmission of thermoelastic waves. At the early stage ($t = 12$), the dilatation is still rather small, but oscillation amplitudes rise with time, with the most noticeable reaction occurring at $t = 18$. The most compressive dilatation happens on the bottom surface ($z \approx 4$ mm), where a strongly negative response indicates localised thermo-mechanical contraction. General wave-like behaviour is maintained, but the dilatation amplitudes near the upper surface are slightly reduced and the oscillations' phase is altered when surface cooling ($\varrho > 0$) is introduced. Time has a greater impact than the cooling coefficient, especially in the deeper tissue region.

Using the exponential Pennes thermoelastic theory (e-PT) for (a) $\varrho = 0$ and (b) $\varrho > 0$, Figure 9 shows how time affects the normalised axial stress ($\hat{\sigma}$) through the skin tissue. Finite-speed thermoelastic wave propagation is indicated by the axial stress's clear wave-like distribution throughout the tissue. The compressive stress is comparatively small at the earliest period ($t = 12$); however, the compressive stress magnitudes increase with increasing time. The deeper tissue region ($z \approx 3 - 4$ mm), where the stress reaches its highest negative values, experiences the largest compressive stresses at $t = 18$. While

maintaining the overall oscillatory behaviour, surface cooling ($\varrho > 0$) modifies the stress profile significantly and lowers the compressive stress close to the upper surface ($z = 0$). The thermo-mechanical response is dominated by time, with deeper tissue showing more noticeable stress evolution than the surface area.

4.3. The Impact of Exposure Time of Laser Radiation

Figures 10–13 show the effects of laser radiation exposure duration (α) on temperature, deflection, dilatation, and axial stress distributions during e-PT of thermoelasticity ($\tau = 5$ s, $t = 15$ s).

Using the exponential Pennes thermoelastic theory (e-PT) for (a) $\varrho = 0$ and (b) $\varrho > 0$, Figure 10 shows how the laser exposure period (α) affects the normalised temperature ($\hat{\theta}$) across the skin tissue. As the laser exposure period drops from $\alpha = 12$ to $\alpha = 9$, the temperature rises, suggesting that shorter exposure times result in a higher thermal reaction. The exponential Pennes model predicts finite-speed heat propagation, which causes a wave-like spatial variation in all temperature profiles. Particularly in the deeper tissue region ($z \approx 3 - 4$ mm), $\alpha = 12$ results in the lowest temperatures, whereas $\alpha = 9$ yields the highest temperatures. Surface cooling ($\varrho > 0$) diminishes the thermal response and marginally lowers the temperature close to the upper surface, but the overall profile and oscillatory behaviour essentially stay the same. Especially in the lower portion of the tissue, the impact of the laser exposure duration is greater than that of the cooling coefficient.

Using the exponential Pennes thermoelastic theory (e-PT) for (a) $\varrho = 0$ and (b) $\varrho > 0$, Figure 11 shows how the laser exposure period (α) affects the normalised axial displacement ($\hat{w}$) across the skin tissue. The propagation of thermoelastic waves is indicated by the axial displacement's oscillatory distribution throughout the tissue. The displacement goes toward larger positive values as the laser exposure period increases from $\alpha = 9$ to $\alpha = 12$, with $\alpha = 12$ exhibiting the largest displacement. Larger negative displacement amplitudes are produced by shorter exposure durations ($\alpha = 9$), especially in the deeper tissue region ($z \approx 3 - 4$ mm). The displacement reaction is very mild in the vicinity of the upper surface and is most noticeable in the bottom portion of the tissue. Surface cooling ($\varrho > 0$) modifies the overall displacement profiles only slightly and diminishes the displacement amplitudes close to the upper surface.

Using the exponential Pennes thermoelastic theory (e-PT) for (a) $\varrho = 0$ and (b) $\varrho > 0$, Figure 12 shows the impact of the laser exposure period (α) on the normalised dilatation ($\hat{\varepsilon}$) across the skin tissue. The propagation of thermoelastic waves is reflected in the dilatation's noticeable oscillating distribution throughout the tissue. A weaker volumetric deformation is shown by the oscillation amplitudes steadily decreasing as the laser exposure time increases from $\alpha = 9$ to $\alpha = 12$. The shortest exposure duration ($\alpha = 9$) results in the highest positive and negative dilatation values, particularly in the deeper tissue region ($z \approx 3 - 4$ mm). While maintaining the rhythmic structure of the response, longer exposure times result in smoother dilatation profiles with smaller peak amplitudes. Surface cooling ($\varrho > 0$) results in small oscillation pattern adjustments and a slight decrease in dilatation amplitudes near the upper surface without changing the overall trend.

Using the exponential Pennes thermoelastic theory (e-PT) for (a) $\varrho = 0$ and (b) $\varrho > 0$, Figure 13 shows how the laser exposure period (α) influences the normalized axial stress ($\hat{\sigma}$) throughout the skin tissue. The axial stress clearly oscillates throughout the tissue, exhibiting the thermoelastic wave behaviour that the exponential model predicts. The compressive stress decreases, and the stress profiles move toward higher (less negative) values as the laser exposure time increases from $\alpha = 9$ to $\alpha = 12$. The shortest exposure duration ($\alpha = 9$) results in the highest compressive stresses, especially in the deeper tissue region ($z \approx 3 - 4$ mm), whereas $\alpha = 12$ yields the lowest compressive stresses. While the stress amplitudes drop with increasing exposure duration, the rhythmic pattern

remains constant throughout. Surface cooling ($\varrho > 0$) causes only tiny variations in the stress distribution without changing the general trend, and it also marginally reduces the stress magnitude near the upper surface.

5. Conclusions

This research presents a generalized thermoelastic investigation of skin tissue exposed to laser radiation employing the exponential Pennes thermoelasticity model. The relationship between blood perfusion, metabolic heat generation, and tissue thermal behaviour is investigated. By adding exponential thermal memory to the traditional Pennes bioheat equation, the proposed formulation explains finite-speed heat transmission and the associated thermo-mechanical response of biological tissue. The governing equations are solved analytically via the Laplace transform method.

The surface temperature decreases, and the thermal gradient steepens when the cooling heat transfer coefficient (ϱ) is increased. The largest thermal memory effect and the most noticeable temperature response are shown by the exponential Pennes thermoelasticity model. Axial displacement is reduced using surface cooling, with the conventional Pennes model showing the greatest reduction. The most important thermo-mechanical response because of thermal memory is predicted using the exponential model. The volumetric deformation is somewhat suppressed by cooling, mostly in the vicinity of the upper surface. The most noticeable oscillatory dilatation, which reflects increased memory effects, is produced by the exponential Pennes model. While the generalized models maintain wave-like stress propagation that is lacking in classical theory, surface cooling slightly reduces the stress amplitude. The strongest thermoelastic stress response is produced using the exponential model.

A time-dependent rise in temperature because of thermal-wave propagation is predicted using the exponential Pennes model. Surface cooling has little effect on the general distribution and mostly lowers the temperature close to the surface. As thermoelastic waves travel, axial displacement grows with time. Without altering its general propagation pattern, surface cooling marginally reduces the displacement. While surface cooling marginally reduces the near-surface response while maintaining the overall oscillatory behaviour, dilatation gradually becomes more noticeable. Thermoelastic wave propagation causes compressive axial stress to increase with time. Surface cooling has a minor impact on the overall stress distribution but marginally lowers the stress close to the surface.

Stronger thermal-wave propagation and higher temperatures are produced by shorter laser exposure durations. With minimal impact on the distribution, surface cooling mostly reduces the temperature close to the surface. Surface cooling only marginally lowers the displacement response's amplitude without changing the propagation pattern; however, laser exposure period has a significant impact. Longer exposure times decrease the amplitude of dilatation, while shorter exposure times increase it. The effect is very slightly attenuated by surface cooling. Longer laser exposures reduce the magnitude of compressive pressures, but shorter exposures increase them. The entire stress field is barely affected by surface cooling.

The results demonstrate that the exponential Pennes model predicts greater thermo-mechanical coupling and more pronounced thermal-wave propagation than the classical, simple, and refined Pennes models. Surface cooling effectively reduces the temperature and slightly attenuates the mechanical fields, but shorter laser exposure times lead to higher temperatures, larger deformations, and stronger compressive stresses. Better physical understanding of non-Fourier bioheat transfer is provided by the proposed analytical model, which may also serve as a useful benchmark for the advancement of laser-based thermal therapeutic and biomedical applications.

https://doi.org/10.3390/ma19234982

Author Contributions: Conceptualization, A.A.A.-R. and A.M.Z.; Methodology, A.A.A.-R. and A.M.Z.; Software, A.A.A.-R.; Validation, A.M.Z.; Formal Analysis, A.A.A.-R.; Investigation, A.A.A.-R. and A.M.Z.; Resources, A.A.A.-R.; Data Curation, A.A.A.-R. and A.M.Z.; Writing—Original Draft, A.A.A.-R. and A.M.Z.; Writing—Review & Editing, A.A.A.-R. and A.M.Z.; Visualization, A.A.A.-R. and A.M.Z.; Supervision, A.M.Z.; Project Administration, A.M.Z.; Funding Acquisition, A.A.A.-R. All authors have read and agreed to the published version of the manuscript.

Funding: This research was funded by King Khalid University, grant number RGP2/570/47.

Institutional Review Board Statement: Not applicable.

Informed Consent Statement: Not applicable.

Data Availability Statement: The original contributions presented in this study are included in the article. Further inquiries can be directed to the corresponding author.

Acknowledgments: The authors extend their appreciation to the Deanship of Research and Graduate Studies at King Khalid University for funding this work through the Large Research Groups Program under grant number RGP2/570/47.

Conflicts of Interest: The authors declare no conflicts of interest.

References

1. Shih, T.-C.; Yuan, P.; Lin, W.-L.; Kou, H.-S. Analytical analysis of the Pennes bioheat transfer equation with sinusoidal heat flux condition on skin surface. *Med. Eng. Phys.* **2007**, *29*, 946–953. https://doi.org/10.1016/j.medengphy.2006.10.008.
2. Ahmadikia, H.; Moradi, A.; Fazlali, R.; Parsa, A.B. Analytical solution of non-Fourier and Fourier bioheat transfer analysis during laser irradiation of skin tissue. *J. Mech. Sci. Technol.* **2012**, *26*, 1937–1947. https://doi.org/10.1007/s12206-012-0404-9.
3. Kundu, B.; Dewanjee, D. A new method for non-Fourier thermal response in a single layer skin tissue. *Case Stud. Therm. Eng.* **2015**, *5*, 79–88. https://doi.org/10.1016/j.csite.2015.02.001.
4. Kengne, E.; Lakhssassi, A. Bioheat transfer problem for one-dimensional spherical biological tissues. *Math. Biosci.* **2015**, *269*, 1–9. https://doi.org/10.1016/j.mbs.2015.08.012.
5. Askarizadeh, H.; Ahmadikia, H. Analytical study on the transient heating of a two-dimensional skin tissue using parabolic and hyperbolic bioheat transfer equations. *Appl. Math. Model.* **2015**, *39*, 3704–3720. https://doi.org/10.1016/j.apm.2014.12.003.
6. Majchrzak, E.; Turchan, Ł.; Dziatkiewicz, J. Modeling of skin tissue heating using the generalized dual phase-lag equation. *Arch. Mech.* **2015**, *67*, 417–437.
7. Kabiri, A.; Talaee, M.R. Analysis of hyperbolic Pennes bioheat equation in perfused homogeneous biological tissue subject to the instantaneous moving heat source. *SN Appl. Sci.* **2021**, *3*, 398. https://doi.org/10.1007/s42452-021-04379-w.
8. Mukaddes, A.M.M.; Shioya, R.; Ogino, M.; Roy, D.; Jaher, R. Finite element-based analysis of bio-heat transfer in human skin burns and afterwards. *Int. J. Comput. Methods* **2021**, *18*, 2041010. https://doi.org/10.1142/S0219876220410108.
9. Sadeghi, B.; Siahpoush, V.; Nikniazi, A. A basic estimation on the light distribution and thermal behavior of the human skin through transfer matrix method coupled with Pennes' bio-heat equation. *Waves Random Complex Media* **2022**, *32*, 1803–1819. https://doi.org/10.1080/17455030.2020.1838666.
10. Tasnim, Z.J.; Nasrin, R. Thermal wave and Pennes' models of bioheat transfer in human skin: A transient comparative analysis. *Heliyon* **2024**, *10*, e40109. https://doi.org/10.1016/j.heliyon.2024.e40109.
11. Akulova, D.V.; Sheremet, M.A. Mathematical simulation of bio-heat transfer in tissues having five layers in the presence of a tumor zone. *Mathematics* **2024**, *12*, 676. https://doi.org/10.3390/math12050676.
12. Ezzat, M.A.; AlSowayan, N.S.; Al-Muhiameed, Z.I.A.; Ezzat, S.M. Fractional modelling of Pennes' bioheat transfer equation. *Heat Mass Transf.* **2014**, *50*, 907–914. https://doi.org/10.1007/s00231-014-1300-x.
13. Cui, Z.J.; Chen, G.D.; Zhang, R. Analytical solution for the time-fractional Pennes bioheat transfer equation on skin tissue. *Adv. Mater. Res.* **2014**, *1049–1050*, 1471–1474. https://doi.org/10.4028/www.scientific.net/AMR.1049-1050.1471.
14. Sarkar, D.; Haji-Sheikh, A.; Jain, A. Temperature distribution in multi-layer skin tissue in presence of a tumor. *Int. J. Heat Mass Transf.* **2015**, *91*, 602–610. https://doi.org/10.1016/j.ijheatmasstransfer.2015.07.089.
15. Ferrás, L.L.; Ford, N.J.; Morgado, M.L.; Nóbrega, J.M.; Rebelo, M.S. Fractional Pennes' bioheat equation: Theoretical and numerical studies. *Fract. Calc. Appl. Anal.* **2015**, *18*, 1080–1106. https://doi.org/10.1515/fca-2015-0062.

16. Yang, J.; Sun, Y. A Space-fractional Pennes bioheat conduction model for skin tissue. *SN Appl. Sci.* **2021**, *3*, 61. https://doi.org/10.1007/s42452-020-04080-4.
17. Tian, M.-L.; Zhang, X.-Y.; Li, X.-F. Thermoviscoelastic response of skin tissue via fractional Pennes bioheat and fractional viscoelasticity. *J. Therm. Stress.* **2024**, *47*, 959–976. https://doi.org/10.1080/01495739.2024.2349910.
18. Tian, M.-L.; Zhang, X.-Y.; Li, X.-F. Thermoviscoelastic response of skin with temperature-dependent thermal properties by generalized fractional viscoelasticity and phase-lag Pennes bioheat conduction. *Arch. Appl. Mech.* **2026**, *96*, 45. https://doi.org/10.1007/s00419-026-03026-3.
19. Askarizadeh, H.; Ahmadikia, H. Analytical analysis of the dual-phase-lag model of bioheat transfer equation during transient heating of skin tissue. *Heat Mass Transf.* **2014**, *50*, 1673–1684. https://doi.org/10.1007/s00231-014-1373-6.
20. Kumar, D.; Kumar, P.; Rai, K. Numerical solution of non-linear dual-phase-lag bioheat transfer equation within skin tissues. *Math. Biosci.* **2017**, *293*, 56–63. https://doi.org/10.1016/j.mbs.2017.08.009.
21. Kumar, D.; Rai, K. Numerical simulation of time fractional dual-phase-lag model of heat transfer within skin tissue during thermal therapy. *J. Therm. Biol.* **2017**, *67*, 49–58. https://doi.org/10.1016/j.jtherbio.2017.05.001.
22. Zhang, Q.; Sun, Y.; Yang, J. Bio-heat response of skin tissue based on three-phase-lag model. *Sci. Rep.* **2020**, *10*, 16421. https://doi.org/10.1038/s41598-020-73590-3.
23. Zhang, Q.; Sun, Y.; Yang, J. Thermoelastic behavior of skin tissue induced by laser irradiation based on the generalized dual-phase lag model. *J. Therm. Biol.* **2021**, *100*, 103038. https://doi.org/10.1016/j.jtherbio.2021.103038.
24. Wang, Y.Z.; Li, M.J.; Liu, D. Analytical analysis of the dual-phase-lag model of bio-heat transfer with pulse boundary heat flux on skin tissue. *Waves Random Complex Media* **2022**, *32*, 1923–1936. https://doi.org/10.1080/17455030.2020.1842552.
25. Al-Lehaibi, E.A.N. Mathematical modelling with the exact solution of three different bioheat conduction models of a skin tissue shocked by thermoelectrical effect. *Int. J. Biomater.* **2023**, *2023*, 3863773. https://doi.org/10.1155/2023/3863773.
26. Rani, S.; Chaudhary, S.; Gill, V.; Sheoran, S.S. Analysis of magneto-thermoelastic plane waves in biological tissue with voids and variable thermal conductivity under dual-phase-lag model. *Heat Transf.* **2026**, *55*, 2696–2712. https://doi.org/10.1002/htj.70219.
27. Salem, M.G.; Abouelregal, A.E.; Elzayady, M.E.; Sedighi, H.M. Biomechanical response of skin tissue under ramp-type heating by incorporating a modified bioheat transfer model and the Atangana–Baleanu fractional operator. *Acta Mech.* **2024**, *235*, 5041–5060. https://doi.org/10.1007/s00707-024-03988-x.
28. Abbas, I.A.; El-Bary, A.A.; Mohamed, A.O. Generalized thermomechanical interaction in two-dimensional skin tissue using eigenvalues approach. *J. Therm. Biol.* **2024**, *119*, 103777. https://doi.org/10.1016/j.jtherbio.2023.103777.
29. Parmar, P.; Mandal, S.; Sarkar, S.P. Effect of moving heat source within the framework of two-temperature higher order lagging phenomena in human skin tissue. *Mech. Solids* **2025**, *60*, 261–277. https://doi.org/10.1134/S0025654424606177.
30. Megahid, S.F.; Abouelregal, A.E.; Sedighi, H.M. Modified Moore–Gibson–Thompson Pennes' bioheat transfer model for a finite biological tissue subjected to harmonic thermal loading. *Mech. Time-Depend. Mater.* **2024**, *28*, 1441–1463. https://doi.org/10.1007/s11043-023-09647-3.
31. Abouelregal, A.E.; Megahid, S.F.; Sedighi, H.M. Thermal effects of electromagnetic radiation on the skin tissue by considering fourth-order MGT bioheat model. *ZAMM J. Appl. Math. Mech./Z. für Angew. Math. und Mech.* **2024**, *104*, e202301085. https://doi.org/10.1002/zamm.202301085.
32. Megahid, S.F. Two-dimensional biothermomechanical effects in a layer of skin tissue exposed to variable thermal loading using a fourth-order MGT model. *Sci. Rep.* **2025**, *15*, 17023. https://doi.org/10.1038/s41598-025-01745-1 1.
33. Bhattacharya, D.; Kanoria, M. Assessing the impact of ramp-type heating on 1D skin tissue behavior with the Moore–Gibson–Thompson heat transfer model. *Arch. Appl. Mech.* **2025**, *95*, 145. https://doi.org/10.1007/s00419-025-02857-w.
34. Mondal, S.; Singh, R.V.; Mukhopadhyay, S. Multi-layer skin tissue modeling with fourth-order Moore-Gibson-Thompson bioheat equation and Eringen's nonlocal elasticity under a moving heat source. *Appl. Math. Model.* **2026**, *156*, 116879. https://doi.org/10.1016/j.apm.2026.116879.
35. Zenkour, A.M.; Saeed, T.; Al-Raezah, A.A. A 1D thermoelastic response of skin tissue due to ramp-type heating via a fractional-order Lord–Shulman model. *J. Comput. Appl. Mech.* **2023**, *54*, 365–377. https://doi.org/10.22059/JCAMECH.2023.364796.871.
36. Zenkour, A.M.; Saeed, T.; Al-Raezah, A.A. Fractional order of refined Lord–Shulman model for a 1D thermoelastic response of skin tissue due to ramp-type heating. *Arch. Appl. Mech.* **2024**, *94*, 989–1003. https://doi.org/10.1007/s00419-024-02561-1.
37. Pennes, H.H. Analysis of tissue and arterial blood temperatures in the resting human forearm. *J. Appl. Physiol.* **1948**, *1*, 93–122. https://doi.org/10.1152/jappl.1948.1.2.93.

38. Zenkour, A.M.; Saeed, T.; Alnefaie, K.M. Analysis of the bio-thermoelasticity response of biological tissues subjected to harmonic heating using a refined Green–Lindsay model. *J. Comput. Appl. Mech.* **2023**, *54*, 588–606. https://doi.org/10.22059/JCAMECH.2023.366508.889.
39. Zenkour, A.M.; Saeed, T.; Al-Raezah, A.A. Refined fractional-order for bio-thermoelastic analysis of skin tissue based upon Green–Lindsay model. *Indian J. Phys.* **2026**, *100*, 2199–2212. https://doi.org/10.1007/s12648-026-03994-w.
40. Zenkour, A.M. Time-shift operators with exponential growth in generalized thermoelasticity. *Waves Random Complex Media* **2026**, *in press*. https://doi.org/10.1080/17455030.2026.2704547.
41. Tung, M.; Trujillo, M.; Molina, J.L.; Rivera, M.; Berjano, E. Modeling the heating of biological tissue based on the hyperbolic heat transfer equation. *Math. Comput. Model.* **2009**, *50*, 665–672. https://doi.org/10.1016/j.mcm.2008.12.023.
42. Alzahrani, F.S.; Abbas, I.A. Analytical estimations of temperature in a living tissue generated by laser irradiation using experimental data. *J. Therm. Biol.* **2019**, *85*, 102421. https://doi.org/10.1016/j.jtherbio.2019.102421.
43. Gardner, C.M.; Jacques, S.L.; Welch, A.J. Light transport in tissue: Accurate expressions for one-dimensional fluence rate and escape function based upon monte carlo simulation. *Lasers Surg. Med.* **1996**, *18*, 129–138. https://doi.org/10.1002/(SICI)1096-9101(1996)18:2<129:AID-LSM2>3.0.CO;2-U.
44. Dubner, H.; Abate, J. Numerical inversion of Laplace transforms by relating them to the finite Fourier cosine transform. *J. ACM* **1968**, *15*, 115–123. https://doi.org/10.1145/321439.321446.

Disclaimer/Publisher's Note: The statements, opinions and data contained in all publications are solely those of the individual author(s) and contributor(s) and not of MDPI and/or the editor(s). MDPI and/or the editor(s) disclaim responsibility for any injury to people or property resulting from any ideas, methods, instructions or products referred to in the content.